

## STRUCTURE OF STATIONARY STRONG IMBALANCED TURBULENCE

A. BERESNYAK, A. LAZARIAN

Dept. of Astronomy, Univ. of Wisconsin, Madison, WI 53706

*Draft version November 20, 2018*

### ABSTRACT

In this paper we systematically study the spectrum and structure of incompressible MHD turbulence by means of high resolution direct numerical simulations. We considered both balanced and imbalanced (cross-helical) cases and simulated sub-Alfvénic as well as trans-Alfvénic turbulence. This paper extends numerics preliminarily reported in Beresnyak & Lazarian 2008. We confirm that driven imbalanced turbulence has a stationary state even for high degrees of imbalance. Our major finding is that the structure of the dominant and subdominant Alfvénic components are notably different. Using the most robust observed quantities, such as the energy ratio, we believe we can reject several existing models of strong imbalanced turbulence.

*Subject headings:* MHD – turbulence – ISM: kinematics and dynamics

### 1. INTRODUCTION

Astrophysical fluids are known to be turbulent from large scales of the order of hundreds of kiloparsecs, as in the case of galaxy clusters (Vogt & Ensslin 2005), to scales as small as hundreds of kilometers. Armstrong et al. (1995) reported a wide range of electron density fluctuations probed by scintillation and scattering techniques. New statistical techniques using Doppler-shifted lines have enabled studies of velocity fluctuations on scales larger than a fraction of a parsec (see Lazarian (2009) and refs. therein). Recent years have been marked by new understanding of the key role that turbulence plays in a number of astrophysical processes (Cho, Lazarian & Vishniac 2003, Elmegreen & Scalo 2004). Most notably, turbulence has drastically changed the paradigms of interstellar medium and molecular cloud evolution (Stone et al 1998, Ostriker et al. 2001, Vasquez-Semadeni et al. 2007, see also review by McKee & Ostriker 2007). Small scale turbulence has been probed by a variety of approaches such as gyrokinetics, Hall MHD and electron MHD (Howes et al 2006, Schekochihin et al 2007, Galtier et al 2003, Cho & Lazarian 2004). This progress calls for better understanding of the fundamentals of turbulence. One reason for doing this is to understand to what extent the turbulence simulated with diffusive computer codes resembles actual turbulence in astrophysical fluids with low diffusivity.

We start with a few general remarks on the relation of fluid dynamics and description of astrophysical fluids. The continuous fluid description has been successful describing a wide range of physical phenomena. In space, due to the presence of ionizing radiation and cosmic rays (CRs) the medium is almost always ionized to some degree, i.e. is a plasma. Although the dynamics of plasma is complicated on small scales, it can be considered well-conducting continuous fluid on large scales and, therefore, Magnetohydrodynamics or MHD is applicable.

One of the most interesting phenomena in fluids is turbulence, a seemingly random stochastic flow which appears spontaneously as long as the microscopic dissipation coefficients such as viscosity or magnetic diffu-

sivity are small (which correspond to large Reynolds or magnetic Reynolds numbers). Turbulence increases dissipation due to so-called turbulent cascade, a nonlinear transfer of energy to smaller scales. As astrophysical fluids are turbulent, this affects dynamics and is manifested in a variety of situations such as reconnection, momentum transfer in accretion disks, etc.

The basic theoretical study of the complicated nonlinear dynamics of turbulence has been concentrated on incompressible turbulence with large Reynolds number (Kolmogorov, 1941). While dissipation in plasma might be much more complex than dissipation in molecular gases<sup>1</sup>, in the asymptotic large Reynolds number flows the “inertial range” fluctuations do not feel the peculiarities of the dissipation. On the other hand, it is often necessary to account for compressibility of the fluid, as it could be significant. An example of which is the interstellar medium which has sonic Mach numbers in a range of 0.1 – 10. In this case the dynamics of Alfvén and slow-mode perturbations on small scales can be considered incompressible (Lithwick & Goldreich 2001), while fast mode has the dynamics of its own (Cho & Lazarian 2002, 2003). On the other hand, even at large scales where the compressibility is significant, one can find the features of incompressible dynamics (see, e.g., Beresnyak, Lazarian & Cho 2005). In other words, the understanding of incompressible MHD turbulence, which is often called Alfvénic turbulence due to the dominant role the Alfvén perturbations play in the cascade, is of utmost importance.

Ideal incompressible MHD equations can be written in the following simple form

$$\partial_t \mathbf{w}^\pm + \hat{S}(\mathbf{w}^\mp \cdot \nabla) \mathbf{w}^\pm = 0,$$

where  $\hat{S}$  is a solenoidal projection operator and Elsasser variables are defined in terms of velocity  $\mathbf{v}$  and magnetic field in velocity units  $\mathbf{b} = \mathbf{B}/(4\pi\rho)^{1/2}$  as  $\mathbf{w}^+ = \mathbf{v} + \mathbf{b}$  and  $\mathbf{w}^- = \mathbf{v} - \mathbf{b}$ . Although fairly idealized, the problem of incompressible MHD turbulence with large Reynolds number has been difficult. First attempts to treat it was

<sup>1</sup> The dissipation in collisionless plasmas has been an area of active research recently, see, e.g. Howes et al 2008 and ref. therein.

an IK model by Iroshnikov (1963) and Kraichnan (1965). They found that the mean magnetic field provided by large scales will, very much unlike hydrodynamics, crucially define the dynamics on small scales. Although this first model was isotropic, it was eventually realized that the dynamics will result in anisotropy (Montgomery & Turner 1981, Shebalin et al 1983, Higdon 1984). This resulted in Goldreich & Sridhar 1995 (henceforth GS95) model which postulated so-called “critical balance”, i.e., maximum anisotropy which is allowed under strong interaction. At the same time, the concept of the dominant perpendicular cascade, that was used in GS95, has been validated in an analytical perturbative theory of so-called weak Alfvénic turbulence (Galtier et al. 2000, 2002)<sup>2</sup>.

While hydrodynamic turbulence have only one energy cascade, the incompressible MHD turbulence has two, due to the exact conservation of the Elsasser (oppositely going wave packets’) “energies”. This can be also formulated as the conservation of total energy and cross-helicity<sup>3</sup>. The situation of zero total cross-helicity has been called “balanced” turbulence as the amount of oppositely moving wavepackets balance each other, the alternative being “imbalanced” turbulence. Most of the above studies concentrated on the balanced case, and, without exception, the GS95 model, which is the strong cascading model with critical balance, can only be kept self-consistent assuming balanced case. The real life turbulence, however, is almost always imbalanced, such as in situations when one has a strong localized source of perturbations (the Sun for solar wind or central engine for AGN jets), but also due to inhomogeneity of energy sources for turbulence (supernovas and stellar winds in the ISM) and the tendency of the decaying turbulence to become increasingly more imbalanced with time. Moreover, the purely balanced MHD Alfvénic turbulence can not be understood as it is, without understanding of the more general imbalanced case. This is due to the fact that turbulence is a stochastic phenomena with all quantities fluctuating and every piece of turbulence at any given time can have imbalance in it. In this respect, while the mean-field Kolmogorov model can be expanded to include intermittency, the mean field GS95 model can not.

Imbalanced turbulence, or “turbulence with non-zero cross-helicity” has been discussed long ago by a number of authors (Dobrovolny et al. 1980, Matthaeus & Montgomery 1980, Grappin et al. 1983, Pouquet et al. 1988, Biskamp 2003 and refs. therein). These papers testified that the non-zero cross-helicity modifies the turbulence. Although these studies correctly reproduced separate cascades for energy and cross-helicity, they were based on then-popular models of MHD turbulence and

<sup>2</sup> Although a successful analytical theory, the weak Alfvénic turbulence can rarely be applied to real-life MHD turbulence as it would require weak, relatively isotropic fluctuations on outer scale and a strong mean field. Even when these conditions are satisfied, the strength of the interaction, which can be estimated as  $\delta v_l L / v_A l$ , where  $L/l$  is the anisotropy of the perturbation, will increase down the cascade and break the applicability of the theory. In real life ISM turbulence the perturbations of the magnetic field are of the order of the mean field which makes the turbulence strong from outer scale inwards. For phenomenological treatment of weak Alfvénic turbulence, see also Lazarian & Vishniac 1999.

<sup>3</sup> The latter,  $\int \mathbf{v} \cdot \mathbf{B} d^3x$  is a quantity conserved in the absence of dissipation.

later it became evident that these models are problematic. For example, the closure theory of isotropic turbulence (Pouquet, Frisch & Leorat 1976) which reproduced IK model can be rejected by both theory and numerics<sup>4</sup>. Another class of models were based on so-called two-dimensional MHD turbulence that, as we now know, is unable to reproduce important properties of the real three-dimensional turbulence, such as critical balance.

Recently several models for the strong imbalanced turbulence have been proposed (e.g., Lithwick, Goldreich & Sridhar 2007, Beresnyak & Lazarian 2008, Chandran 2008). As long as the full self-contained analytical model for strong turbulence continues to elude discovery, direct numerical simulations (DNS) will be an inspiration and guidance to theorists. While the Reynolds numbers in those simulations are fairly modest (800-4000 are the best to-date), some of the robust quantities can be measured and used as a guidance to reject theories. While in this paper we are fully aware of these limitations, we present the most robust statistical measures, such as total energies, dissipation rates and second-order structure function (or its equivalent, the spectrum) and the anisotropy derived from it. We leave the study of higher order statistics (and intermittency) to the future studies. Our paper is written on the premise that one cannot fully *confirm* a model using three-dimensional DNS due to their fairly modest resolution, but from these DNS one can collect enough numerical evidence to *reject* a model.

This paper expands parameter space of the preliminary numerical results reported in Beresnyak & Lazarian (2008a). A short introduction into theories of imbalanced turbulence is in §2. Numerical code, the simulation setup, and the establishment of the stationary state are explained in §3. The discussion of the structure function calculated parallel to the magnetic field (parallel SF), a quantity which is a key for understanding statistical anisotropy of MHD turbulence is given in §4. In this section we explain various methods to define the local guiding field and the influence to the measurement of the parallel SF. Scale-dependent anisotropies derived from structure functions as well as power spectra are described in §5. Polarization alignment briefly discussed in §6. Final comparison with models as well as observational data are in §7. We summarize our findings in §8.

## 2. THEORETICAL CONSIDERATIONS

The original GS95 model was based on the renormalization rule for Alfvén wave’s frequency called “critical balance”. The necessity of such renormalization can be seen from a rigorous theory of weak Alfvénic turbulence (Galtier et al 2000, 2002) that predicts so-called “perpendicular cascade”, i.e. the result that nonlinear interaction of Alfvénic waves conserve these wave’s frequencies and only transverse structure of the wave packet is affected. As perpendicular cascade proceeds to small scales, the applicability of weak interaction breaks down, and Alfvénic turbulence becomes strong. In this situation GS95 assumed that the frequency of

<sup>4</sup> The artificial term for “relaxation of triple correlations”, that was necessary to uphold local isotropy in this model, happen to be *larger* than real physical nonlinear interaction. Also numerics show that MHD turbulence is locally anisotropic (Cho & Vishniac 2000, Maron & Goldreich 2001, Cho, Lazarian & Vishniac 2002)

the wavepacket can not be smaller than the inverse lifetime of the wavepacket, estimated from nonlinear interaction. In their closure model GS95 have an explicit ad-hoc term that allows for the increase of the wave frequency. The scale-dependency of this term is based on the assumption of turbulence locality (i.e. there is one characteristic amplitude of perturbation pertaining to each scale). In the imbalanced case, however, we have two such characteristic amplitudes and the choice for frequency renormalization becomes unclear (GS95)<sup>5</sup>. Any theory of strong imbalanced turbulence, which is qualified for serious consideration, must deal with this problem. Let us first demonstrate that a direct generalization of GS95 for imbalanced case does not work, namely if we assume that the frequency renormalization for one wavepacket is determined by the amplitude of the oppositely moving wavepacket. Indeed, in this situation the wave with small amplitude (say,  $w^-$ ) may only weakly perturb large amplitude wave  $w^+$  and the frequency of cascaded  $w^+$  will conserve. On the other hand,  $w^+$  may strongly perturb  $w^-$  and  $w^-$ 's frequency will be determined as  $w_1^+/l^6$ . This creates an inconsistency of the local cascade where both wavepackets must have comparable parallel and perpendicular scales. In order to deal with this fundamental inconsistency, a new physical assumption must be adopted. Due to this fact, in the paper we mostly discuss three models of strong imbalanced turbulence, Lithwick, Goldreich & Sridhar (2007) (LGS07), Beresnyak & Lazarian (2008a) (BL08a), Chandran (2008) (C08), that clearly state: a) the problem above; b) the new physical assumptions being adopted; c) an internally consistent physical model that follows from these assumptions and d) the full predictions of the turbulence spectra and anisotropy. In the discussion section of this paper we also mention other models that claim to have predictions on the strong imbalanced turbulence. We test these incomplete models by comparison with our numerics whenever possible.

### 2.1. LGS07 and C08 models

LGS07 resolve the inconsistency explained above by assuming that the strong wave  $w^+$  is also cascaded strongly and its frequency is simply equal to the frequency of the weak wave, i.e. the critical balance for strong wave uses the amplitude of the strong wave itself ( $w^+ \Lambda = v_A \lambda$ ). In other words, the anisotropies of the waves are identical. The formulae for energy cascading are strong cascading formulae, i.e.

$$\epsilon^\mp = \frac{(w^\mp(\lambda))^2 w^\pm(\lambda)}{\lambda}.$$

This lead to the prediction  $w^+/w^- = \epsilon^+/\epsilon^-$ . However, this prediction, together with assumption of the locality

<sup>5</sup> We assume that imbalanced turbulence is “strong” as long as the applicability of weak Alfvénic turbulence breaks down. This requires that at least one component is perturbed strongly. In the imbalanced turbulence the amplitude of the dominant component is larger, so that in the transition to strong regime the applicability of weak cascading of the subdominant component breaks down first.

<sup>6</sup> Throughout this paper we assume that  $w^+$  is the larger-amplitude wave. This choice, however, is purely arbitrary and corresponds to the choice of positive versus negative total cross-helicity.

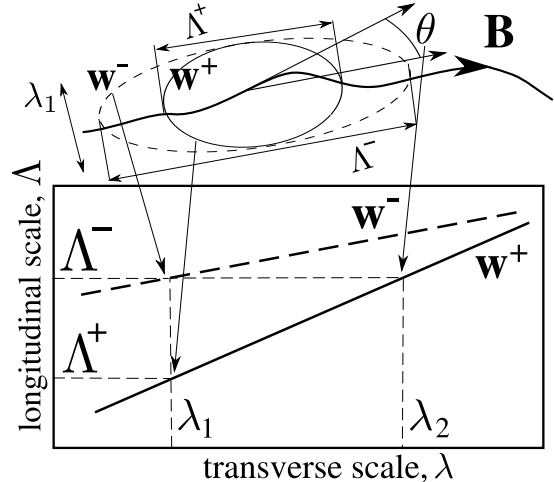


FIG. 1.— Upper: a  $w^+$  wavepacket, produced by cascading by  $w^-$  wavepacket is aligned with respect to  $w^-$  wavepacket, but misaligned with respect to the local mean field on scale  $\lambda_1$ , by the angle  $\theta$ . Lower: the longitudinal scale  $\Lambda$  of the wavepackets, as a function of their transverse scale,  $\lambda$ ;  $\Lambda^+$ ,  $\Lambda^-$ ,  $\lambda_1$ ,  $\lambda_2$  are the notations used in this paper. Modified from BL08a.

of cascading, lead to a contradiction on viscous scale<sup>7</sup> where the nonlinear cascading rates must smoothly transit into viscous dissipation rates. This require  $w^+ = w^-$  on the dissipation scale, so called “pinning” (Lithwick & Goldreich 2003).

C08 is a complicated quantitative theory of advection-diffusion cascading that have several rules to determine the diffusion of the waves in the parallel direction, which are analogous to the frequency renormalization of GS95. In effect, in the case of strong turbulence, the C08 rules lead to equal or very close anisotropies for both waves. Unlike LGS07, however, C08 does not have a strong cascading for both waves, but (again, in effect) it has:

$$\epsilon^\mp = A^\mp \frac{(w^\mp(\lambda))^2 w^+(\lambda)}{\lambda},$$

where the coefficients  $A^\pm$  depend on the spectral slopes of  $w^\mp$ . Although the theory of C08 do not explicitly assume local cascading, in effect it produces such a locality as long as the ratio of dissipation rates (energy fluxes)  $\epsilon^+/\epsilon^-$  is not very large (the critical value is around two), therefore C08 also requires pinning on the viscous scale.

### 2.2. BL08 model

BL08a relaxes the assumption of local cascading for the strong component  $w^+$ , while saying the  $w^-$  is cascaded in a GS95-like way. In BL08a picture the waves have different anisotropies (see Fig. 1) and the  $w^+$  wave actually have smaller anisotropy than  $w^-$ , which is opposite to what a naive application of critical balance would predict. The anisotropies of the waves are determined by

$$w^+(\lambda_1) \Lambda^-(\lambda_1) = v_A \lambda_1, \quad (1)$$

$$w^+(\lambda_2) \Lambda^+(\lambda^*) = v_A \lambda_1, \quad (2)$$

where  $\lambda^* = \sqrt{\lambda_1 \lambda_2}$ , and the energy cascading is determined by weak cascading of the dominant wave and strong cascading of the subdominant wave:

<sup>7</sup> LGS07 does not discuss transition to viscous scales.

$$\epsilon^+ = \frac{(w^+(\lambda_2))^2 w^-(\lambda_1)}{\lambda_1} \cdot \frac{w^-(\lambda_1) \Lambda^-(\lambda_1)}{v_A \lambda_1} \cdot f(\lambda_1/\lambda_2), \quad (3)$$

$$\epsilon^- = \frac{(w^-(\lambda_1))^2 w^+(\lambda_1)}{\lambda_1}. \quad (4)$$

One of the interesting properties of BL08a model is that, unlike LGS07 and C08, it does not produce self-similar (power-law) solutions when turbulence is driven with the same anisotropy for  $w^+$  and  $w^-$  on the outer scale. BL08a, however, claim that, on sufficiently small scales, the initial non-power-law solution will transit into asymptotic power law solution that has  $\Lambda_0^-/\Lambda_0^+ = \epsilon^+/\epsilon^-$  and  $\lambda_2/\lambda_1 = (\epsilon^+/\epsilon^-)^{3/2}$ . The range of scales for the transition region was not specified by BL08a, but it was assumed that larger imbalance will require larger transition region.

### 3. NUMERICAL SETUP

Incompressible MHD equations with dissipation and driving are,

$$\partial_t \mathbf{w}^\pm + \hat{S}(\mathbf{w}^\mp \cdot \nabla) \mathbf{w}^\pm = -\nu_n (-\nabla^2)^n \mathbf{w}^\pm + \mathbf{f}^\pm, \quad (1)$$

where  $n$  is an order of hyperdiffusion, and  $\mathbf{f}^\pm$  is the driving force, whose rms values in arbitrary units are presented in Table 1. These equations were solved by the code which is similar to one in Cho & Vishniac (2001). The differences include introduction of Elsasser driving, the handling of arbitrary physical sizes of the box, regardless of numerical resolution (i.e. elongated boxes for sub-Alfvénic turbulence) and significant improvements in numerical efficiency. Our code is pseudospectral, i.e., it solves ODE in time with finite difference for each spacial Fourier harmonic, the nonlinear term being calculated in real space, while solenoidal projection and dissipation terms were applied in Fourier space. Pseudospectral methods in fluid dynamics has been known since 80-s (Canuto et al, 1988). The strong point of pseudospectral codes is that they allow precise control over dissipation and exact incompressibility. Not only does it relieve worries with respect to grid effects and numerical dissipation, but it also makes possible the use of hyperviscosity and hyperdiffusivity which extends useful inertial interval although at the expense of increased (compared to physical viscosity) bottleneck effect and a different form of the spectral slopes (for more discussion on spectral slopes, see Beresnyak & Lazarian 2008b (BL08b)). The simple version of our pseudospectral code uses periodic boundary conditions. This necessitates a discussion on whether this introduces artificial effects. In the subsequent sections we show that a) our numerical boxes have enough parallel size to allow for eddies of the largest parallel size, dictated by dynamics, to exist; b) at any given time our box contains large number of independent turbulent realizations ( $\sim 40$ ) c) the dynamical time of the eddy is several times smaller than it takes the eddy to cross the box boundaries.

#### 3.1. Choice of physical dimensions, numerical resolution and driving

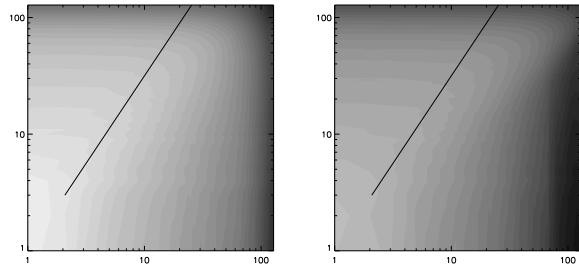


FIG. 2.— Two-dimensional energy spectrum in sub-Alfvénic and trans-Alfvénic case. For sub-Alfvénic case the abscissa  $k_x$  is scaled with  $1/M_A$  factor. The dashed line indicates GS95  $k_{\parallel} \sim k_{\perp}^{2/3}$  anisotropy.

The sub-Alfvénic turbulence, where the perturbation strengths  $w^\pm$  are smaller than  $v_A$  is either weak or strong but anisotropic. The critical anisotropy is determined by the breakdown of the applicability of weak MHD turbulence which happens when  $k_{\parallel} v_A / k_{\perp} \delta v \sim 1$ . In most of our simulations we drive turbulence on outer scale with the same anisotropy for both wave species, so this breakdown is determined by  $\delta v$  of the strong wave. We drive turbulence on outer scale in such a manner that the strong interaction establishes on the outer scale. Also, we provided driving for  $k = 2..3.5$  which means that the maximum eddy size is several times smaller than the box. This is to ensure that the first turbulent scales  $k \approx 4$  have more than enough space in parallel direction in case that we did not estimate the transition into strong interaction regime correctly and the parallel scale of the cascaded eddies is longer than we expected. The results from §5, however, suggest that our choice was correct, with the largest coherent eddy size being around 1/4 of the box size in both parallel and perpendicular directions. We used fully predetermined stochastic driving in both Elsasser variables<sup>8</sup> with a certain amplitude of the force ( $f^\pm$ , see Table 1), so the energy input wasn't strictly controlled by the forcing, but rather was calculated during the simulation<sup>9</sup>. In addition, we developed a driving which ensures constant energy input for both components, these tests confirm properties of the imbalanced turbulence that were obtained with fully stochastic driving. We used the latter for most of our simulations.

In studying sub-Alfvénic turbulence we adopted the approach to increase  $v_A$  by increasing  $B_0$  and increase the parallel physical size of the box  $L$  by the same fac-

<sup>8</sup> Elsasser driving is a preferred way to study inertial range of subAlfvénic turbulence as it simulates the supply of Elsasser energies from larger eddies of a realistic turbulence. It is important to remember that kinetic and magnetic energies are not separately conserved by MHD equations. So when one has a pure velocity driving in a simulation with mean field (as in Cho & Vishniac 2001), he will generate approximately as much magnetic perturbations due to the Alfvén effect, the result being two Alfvén or pseudo-Alfvén waves propagating in opposite directions. These waves, however, would have an artificial correlation (reflected by the fact that at  $t = 0$   $\mathbf{b} = \mathbf{0}$ ). In order to use all degrees of freedom and have better stochasticity one has to drive  $\mathbf{w}^+$  and  $\mathbf{w}^-$  independently. The mechanisms by which the outer scales of a realistic, say, ISM turbulence are driven are briefly discussed in §7.3 and §7.4.

<sup>9</sup> Some simulations of *hydrodynamic* turbulence used negative viscosity on large scales to drive turbulence. In MHD this somewhat unphysical approach does not work because in this case even in the balanced simulations imbalance spontaneously occur and continue to increase without limit.

tor  $1/M_A$  without changing the equilibrium value of  $\delta v$ , so that strong interaction timescale  $\lambda/\delta v$  stays constant and similarly the eddy transverse time  $\Lambda/v_A$  also stays constant. Alternatively, one can keep  $B_0$  constant, but decrease  $\delta v$ , but in this case the timescales of sub- and trans-Alfvénic turbulence will be different. Also it is harder to tune the equilibrium  $\delta v$ , rather than  $B_0$  and  $L$ .

Note, that one can naively assume that due to GS95 anisotropy one needs lower numerical resolution in the parallel direction, approximately by the ratio of the anisotropies on the driving scale and on the dissipation scale, which is  $(k_{\perp diss}/k_{\perp driv})^{1/3}$  in the GS95 model, and can be a number between 2 and 4 in a high resolution MHD simulation. For instance, Bigot, Galtier & Politano 2008 used  $512 \times 512 \times 64$  numerical resolution. On the second thought this approach is not evident, since the highest values of  $k_{\parallel}$  in the *global reference frame* will be determined by field wandering on the outer scale. In other words the anisotropy in the global frame will be approximately scale-independent and the ratios of  $k_{\perp diss}/k_{\perp driv}$  and  $k_{\parallel diss}/k_{\parallel driv}$  will be almost equal, which necessitates the use of  $N_x N_x N_x$  numerical resolution, i.e. cubes, for both elongated ( $M_A < 1$ ) and cubic ( $M_A \approx 1$ ) physical boxes.

We confirmed this by plotting the parallel and perpendicular spectra in the global frame and saw that the parallel spectrum protrude to almost as far as  $k_{\perp max}/M_A$ . Fig. 2 shows how energy is distributed on the two-dimensional  $k_{\parallel}, k_{\perp}$  plane (global reference frame). We see that while most of the energy is in GS95 cone, there is also plenty of energy outside of it, especially in the upper right corner which correspond to maximum space frequencies in both parallel and perpendicular direction. If one decide to significantly cut numerical resolution in parallel direction he/she would incorrectly describe the dynamics on small scales. In only one of our simulations, A1 (see Table 1) we were able to cut parallel resolution by a moderate factor of 1.5 without sacrificing small parallel scales, due to the relative lack of energy in parallel direction in this particular *balanced sub-Alfvénic* case. In all other simulations such a reduction was not possible because most of the k-space was filled with energy. We note that Müller & Grappin (2005), by using  $1024 \times 1024 \times 256$  resolution in their balanced sub-Alfvénic simulations have reduced parallel resolution by a factor of 4, which is, most likely, too large.

For all simulations A1-A8 we used hyperviscosity and hyperdiffusivity of 6th order ( $k^6$ ). This choice was necessitated by the nature of imbalanced turbulence which has shorter inertial range for dominant wave due to fairly large cascading timescale of this wave (see §2). With currently available numerical resolutions one cannot see an inertial interval of the strong wave in a simulation with large imbalance and real ( $k^2$ ) diffusivity. Unfortunately, due to the bottleneck effect, hyperdiffusion have affected spectral slopes, although the effect on anisotropy was much less. We refer to BL08b for a comparison of turbulent simulations with normal and hyperviscosity. Due to hyperviscosity the dissipation scale was fairly small, the dissipation cutoff was around  $k = 200$  (with Nyquist frequency of 384) for balanced simulations and about the same for weak component in imbalanced simu-

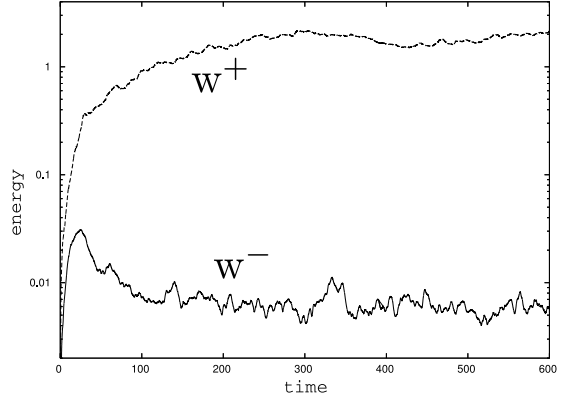


FIG. 3.— The energy evolution in time for both Alfvénic modes for  $\epsilon^+/\epsilon^- = 12$ .

lations. The strong component for the most imbalanced simulations A7 and A8 had a cutoff around  $k = 100$  (Fig. 9). Due to hyperviscosity we can not uniquely define a Reynolds number of our simulations, however viscous simulations with  $Re = Re_m \approx 6000$  could provide turbulence inertial ranges that are similar to ours.

Once we have chosen the geometry of our simulation and figured out the extend of the perturbations on the spectral plane, the choice of timestep becomes evident. On one hand, for the dissipation term we use integration technique (Cho & Vishniac 2000, see also Maron & Goldreich 2001), and since we don't worry too much about the precision of the dissipation term, it doesn't limit the timestep. On the other hand, the general nonlinear term, containing both  $B_0$  and  $\delta v$  can be seen as the sum of linear advection term with velocity  $v_A$  and nonlinear advection with  $\delta v$ ,  $\delta b$ , etc. In turbulence, that is driven to be strong on the outer scale, these terms will be of the same order if we refer to the outer scale, i.e. the terms will be  $v_A \delta v k_{\perp driv}$  and  $\delta v \delta v k_{\parallel driv}$ . On the dissipation scale these terms will be determined by  $v_A \delta v k_{\perp diss}$  and  $\delta v \delta v k_{\parallel diss}$ , which are, by the argument in the above paragraph, again on the same order. So we can just use linear advection behavior to estimate the timestep. This behavior in k-space is, essentially, a rotation of the phase of the wave, in a manner of  $\exp(ik_{\parallel} v_A t)$ . In order to reproduce this rotation numerically we need  $k_{\parallel max} v_A \Delta t$  to be smaller than unity, such as around 0.1, so that the code stays stable, since we don't need good precision beyond the dissipation scale where there is no energy.

The average dissipation rates  $\epsilon^{\pm}$  reported in Table 1 were calculated using a sum of the work done to the Elsasser fields, i.e. we summed  $(\mathbf{w}^{\pm} + \mathbf{f}^{\pm} dt) \cdot \mathbf{f}^{\pm} dt$  at every timestep. As our code (its nonlinear part) was energy conserving, we assume that the same amount of energy was, on average, lost to the dissipation term. We also confirmed these values of  $\epsilon^{\pm}$  by using third order Chandrasekhar-Politano-Pouquet structure functions (see, e.g., Biskamp 2003), which quantify nonlinear energy transfer.

### 3.2. Establishment of the stationary state

One of the goals of this paper is to demonstrate that a stationary state exists for imbalanced turbulence with rather high degree of imbalance. Note, that the local model of weak Alfvénic turbulence work for imbalances

Run	$n_x \cdot n_y \cdot n_z$	x:y:z	$B_0$	$f^+$	$f^-$	$\Delta t_0$	$\Delta t$	$\Delta t_1$	Ncubes	$f^+/f^-$	$\epsilon^+/\epsilon^-$	$(w^+)^2/(w^-)^2$
A1	$512 \cdot 768^2$	10:1:1	10	0.4	0.4	186	10	4.0	3	1	1	1
A2	$768^3$	1:1:1	1	0.44	0.44	186	10	4.0	3	1	1	1
A3	$768^3$	10:1:1	10	0.34	0.255	500	26	8.0	6	1.33	2.0	$5.5 \pm 1.0$
A4	$768^3$	1:1:1	1	0.4	0.3	180	22	8.0	5	1.33	1.7	$3.9 \pm 0.3$
A5	$768^3$	10:1:1	10	0.16	0.08	154	33	12.0	6	2	7.4	$145 \pm 10$
A6	$768^3$	1:1:1	1	0.19	0.095	40	33	12.0	5	2	5.4	$90 \pm 10$
A7	$768^3$	10:1:1	10	0.06	0.02	204	63	21.0	8	3	16	$1150 \pm 100$
A8	$768^3$	1:1:1	1	0.075	0.025	160	63	21.0	8	3	12	$1100 \pm 100$

TABLE 1

SIMULATIONS OF STRONG SUB-ALFVÉNIC ( $B_0 = 10$ ) AND TRANS-ALFVÉNIC ( $B_0 = 1$ ) TURBULENT FLOWS. A1 AND A2 ARE BALANCED SIMULATIONS FOR COMPARISON WITH THE REST. A3 AND A4 ARE SLIGHTLY IMBALANCED, A5 AND A6 ARE STRONGLY IMBALANCED AND A7 AND A8 ARE VERY STRONGLY IMBALANCED.  $\Delta t_0$  IS THE DURATION OF PRIOR LOW RESOLUTION RUN IN CODE UNITS,  $\Delta t$  IS THE DURATION OF THE HIGH RESOLUTION RUN, INTERVAL  $\Delta t_1$  IN THE END OF HIGH-RESOLUTION RUN WAS USED FOR DATA ANALYSIS.

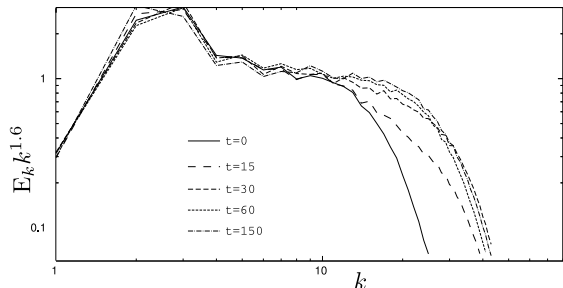


FIG. 4.— Spectrum relaxation towards stationary state. The resolution of the experiment was increased from  $128^3$  to  $256^3$ . Only the spectrum of the dominant wave is shown. The lines correspond to  $t = 15, 30, 60, 150$ .

of no more than  $\epsilon^+/\epsilon^- = 2$  (Galtier 2000, Lithwick & Goldreich 2003), and the model of strong imbalance turbulence of C08 also require similar limitation.

The highest imbalance we attempted in our simulation of  $\epsilon^+/\epsilon^- = 16$  was essentially limited by the long times of establishment of the stationary state. Note that according to BL08a the dominant wave is cascaded weakly and its cascading times could be very large. Fig. 3 shows the total energy evolution for both modes for the  $\epsilon^+/\epsilon^- = 16$  case<sup>10</sup>. The full relaxation towards stationary state required around 300 Alfvén times or 50 crossing times.

As high imbalanced simulations proved to be so computationally expensive, we made a second experiment, which was to take the initial state that was already stationary and to increase the numerical resolution, which allow the spectrum to extend to larger wavenumbers. Note, that our forcing, although stochastic, was predetermined for each particular simulation and did not depend on numerical resolution. Now the question was how fast the spectra will relax to their stationary states. It turned out that the spectrum of the sub-dominant wave relaxed almost instantly, in a one dynamical time, which is consistent with BL08a, while for the dominant wave the relaxation time was long. Note, the the dynamic

<sup>10</sup> Time was measured in Alfvénic units, but the size of the box was  $2\pi$ , thus  $2\pi$  was the time for an eddy to cross the box. The time for the largest turbulent eddy to cross itself, and also the largest eddy dynamical time ( $L/v$ ) was around unity, because the size of the largest eddy was a fraction of around 0.2 or 0.3 of the cube size (see Figs. 7 and 8).

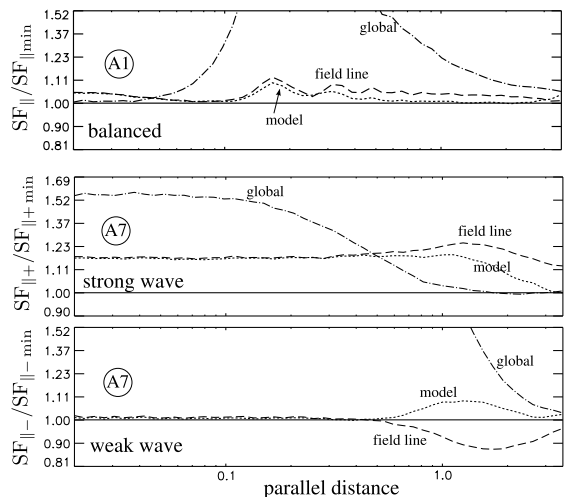


FIG. 5.— The ratio between parallel SFs calculated with different definition of the local field. Upper plot is for balanced simulation, while two lower plots are for strongly imbalanced simulation. The reference SF is “minimum” one described in the text. The dotted line is “model-dependent” SF, dashed line is for “following a field line” method and the dotted-dashed line is for constant global mean field.

(kinetic) timescale  $l/v$  for this region of  $k$ -space for the strong wave was rather small, around 0.3. The relaxation process is shown on Fig. 4. It took  $\delta t \approx 60$  to get reasonably close to the stationary state. We considered this experiment a success and used the technique of increasing resolution to save computational time.

We also studied long-term evolution of nearly-balanced case when we allowed the low-resolution version of A3 to evolve for 500 time units. We didn’t notice any long-term trends either in three-dimensional spectrum or in any other quantities during this run.

#### 4. PARALLEL STRUCTURE FUNCTION

Unlike perpendicular structure function which is largely insensitive to the direction of the local field, the definition of the local field strongly affect the parallel structure function, which, in turn, determines the shape of the turbulent eddy. Since the latter is the major object of study in this paper we feel that the proper explanation of this point is due.

The simplest way to define parallel structure function,

$SF_{\parallel}$ , is to take samples along the *global mean field*. This definition is, however, fairly bad, as it does not take into account field wandering. We expect  $SF_{\parallel}$ , defined in such way, along with perpendicular structure function to reflect the anisotropy in the *global frame*, which, by the effects of field wandering, as we argued in §2, will be similar to the outer scale anisotropy. Therefore, such definition will effectively erase *scale-dependent anisotropy* which is the property of GS95-type models.

Another way is to define local magnetic field by averaging over some scale  $\lambda$ . In this way the parallel structure function become a function of two scales, such as

$$SF_{\parallel}^2(w^{\pm}, \Lambda, \lambda) = \langle (w^{\pm}(\mathbf{r} - \Lambda \mathbf{b}_{\lambda}/b_{\lambda}) - w^{\pm}(\mathbf{r}))^2 \rangle_{\mathbf{r}},$$

where  $\mathbf{b}_{\lambda}$  is the magnetic field averaged over scale  $\lambda$ . We use Gaussian averaging defined as  $\mathbf{b}_{\lambda} = 1/\lambda\sqrt{2\pi} \int \mathbf{b}(\mathbf{r} - \mathbf{R}) \exp(-R^2/2\lambda^2) d\mathbf{R}$ . In order to reduce such a SF to a function of only  $\Lambda$  one can introduce a dependence between  $\Lambda$  and  $\lambda$ , and plug in the  $\lambda = f(\Lambda)$  in the above equation. This definition of  $SF_{\parallel}$  will be a *model-dependent* though.

$$SF_{\parallel model}^2(w^{\pm}, \Lambda) = SF_{\parallel}^2(w^{\pm}, \Lambda, f(\Lambda))$$

For the balanced turbulence the anisotropy was measured to be close to the one predicted by GS95, i.e.  $\Lambda \sim \lambda^{2/3}$ . One can, therefore, introduce a *reasonable* model-dependent  $SF_{\parallel}$  as taking  $f(x) = const \cdot x^{3/2}$ , where the constant depend on the outer scale of the simulation. As we show below, this definition is almost perfect for balanced turbulence, but the question is whether it does equally well for the imbalanced case.

Let us consider some *model-independent* ways to determine  $SF_{\parallel}$ . Apparently, the first definition using global field is model-independent, but fairly bad, it correspond to taking averaging  $\lambda = \infty$ . One can also take  $\lambda = 0$ , i.e. always use local field without any averaging. An interesting model-independent method was used in Maron & Goldreich 2001, where two points were chosen to lie on the same magnetic field line. The distance  $\Lambda$  was also calculated along the line.

When we look for anisotropy we normally want to obtain lower values of  $SF_{\parallel}$ . According to the eddy ansatz, outlined in §2, we receive *lower* values of  $|w^{\pm}(\mathbf{r} - \Lambda \mathbf{n}(\mathbf{r})) - w^{\pm}(\mathbf{r})|$ , where  $\mathbf{n}$  is a unit vector along the eddy. Therefore, the averaging of the field that provides *minimum* values of  $SF_{\parallel}$  approximates the direction of the eddy alignment better, provided that there is a connection between the field direction and eddy alignment (if there is no such connection, there will be no dependence on the averaging scale  $\lambda$ ).

So, another model independent way to define  $SF_{\parallel}$  will be

$$SF_{\parallel min}^2(w^{\pm}, \Lambda) = \min_{\lambda} SF_{\parallel}^2(w^{\pm}, \Lambda, \lambda).$$

This definition not only provides us with the value of  $SF_{\parallel}$ , but, giving  $\lambda$  at which minimum is achieved, gives us a hint to how eddies are aligned with respect to the magnetic field.

Fig. 5 shows a comparison between different methods to calculate parallel SF. We plotted them relative to

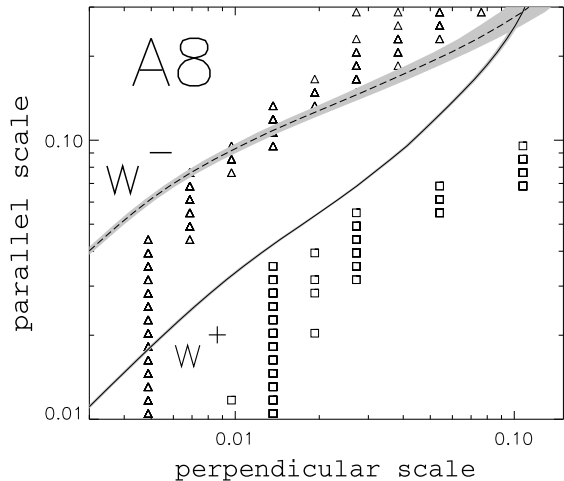


FIG. 6.— This plot shows values of  $\lambda_{avr}$  at which the minimum of the parallel structure function is reached. Triangles show perpendicular scales  $\lambda_{avr}$  at which the minimum of  $SF_{\parallel}^2(w^-, \Lambda)$  is reached, while squares show perpendicular averaging scales at which the minimum of  $SF_{\parallel}^2(w^+, \Lambda)$  is reached. Solid and dotted lines indicate  $w^+$  and  $w^-$  eddies’ anisotropy which are defined in §5 and presented on Fig. 11.

$SF_{\parallel min}^2$ . In the balanced case the three methods – “minimal”, “following the field line” and “model-dependent” work very well, while “global field” method doesn’t work. The latter confirms that turbulent eddies are aligned with respect to local field, not the global field (Cho & Vishniac 2000). In the imbalanced case the situation is more complicated. For the weak component all three “good” methods work very well, while for the strong wave there is a systematic error for all methods, except “minimal”. This is due to the fact that in the imbalanced turbulence the strong component ( $w^+$ ) eddies are aligned with respect to much larger scales of the magnetic field (see §2.2). Since most magnetic field perturbation is provided by the strong wave, it follows that the strong field eddies are aligned with their own field on a larger scale. This directly confirms the prediction of BL08a model. On the bottom panel of Fig. 5 the “field line” method gives values that are smaller than “minimal” method. This is due to the fact that in the field line method we measured the distance along magnetic field, and the physical distance was actually shorter, this allowed for smaller than  $SF_{\parallel min}^2$  values on the outer scale where the difference between straight-line distance and along-the-field-line distance is significant.

It turns out (Fig. 6) that the averaging scale at which minimum of parallel structure is reached for weak wave approximately corresponded to its anisotropy, which is consistent with strong cascading hypothesis. But for strong wave this averaging scale is *larger* than the perpendicular scale dictated by anisotropy. In other words, the eddies of the strong wave are aligned with respect to the magnetic field which is averaged on *larger scale* than the eddy’s own perpendicular scale. This is consistent with the BL08a model.

## 5. SPECTRA AND ANISOTROPIES

We calculated two-dimensional (depending on parallel and perpendicular distances) second order structure functions with respect to the local field using “model

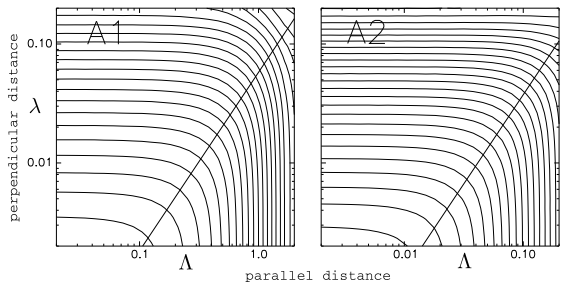


FIG. 7.— Comparison of the SFs from trans-Alfvénic (left) and sub-Alfvénic (right) balanced simulations. Note the difference in x axis between two plots which indicates that A1 is approximately 10 times more anisotropic. Contours indicate SF levels, solid line is a demonstration of GS95  $\Lambda \sim \lambda^{2/3}$  law

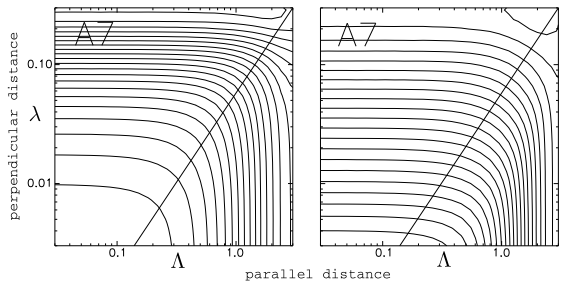


FIG. 8.— Comparison of the SFs from dominant (left) and sub-dominant (right) Alfvénic waves from  $\epsilon^+/\epsilon^- = 16$  imbalanced simulations. The anisotropies of components are notably different. The solid line is the GS95  $\Lambda \sim \lambda^{2/3}$  law

dependent” definition of the local field from previous section. Although this method slightly underestimates anisotropy, according to Fig. 5, it works fairly well. The structure functions were calculated using all available “stationary state” datacubes, i.e. were averaged over time. The contours of these SFs for balanced simulations A1 and A2 are presented on Fig. 7 and for imbalanced simulation A7 on Fig. 8. Fig. 7 shows SFs for total energy i.e. it is summed over  $w^+$  and  $w^-$ . These figures basically validate our assumptions from §3 regarding physical and computational dimensions of the box. We see that, according to expectations, trans-Alfvénic A2 is almost isotropic on outer scale but becomes progressively anisotropic towards small scales, while, as we expected, sub-Alfvénic A1 has approximately 10:1 anisotropy on outer scale, and increases towards small scales. If we decrease anisotropy of A1 by a factor of 10 by rescaling x-axis we almost reproduce A2, the difference is mostly being on the outer scale (this difference is easier to see on Fig 10.). Fig. 8 shows SFs for two separate components  $w^+$  and  $w^-$  in the strongly imbalanced case of A7. The anisotropy on outer scale is approximately 10:1 for both components, which validates our choice of computational box. This anisotropy increases towards small scale, but in a different fashion for each component. We see the anisotropy of strong wave is almost 5 times smaller on dissipation scales.

Fig. 9 shows so-called three-dimensional angle-summed spectra for both components in all simulations. These spectra are obtained by summation of spectra over solid angle for all wavevectors with the same magnitude  $k$ . It can be related to three-dimensional angle-averaged spectra by dividing by  $k^2$ . In the sub-Alfvénic cases A1, A3, A5 and A7, this spectrum is almost identical to the so-

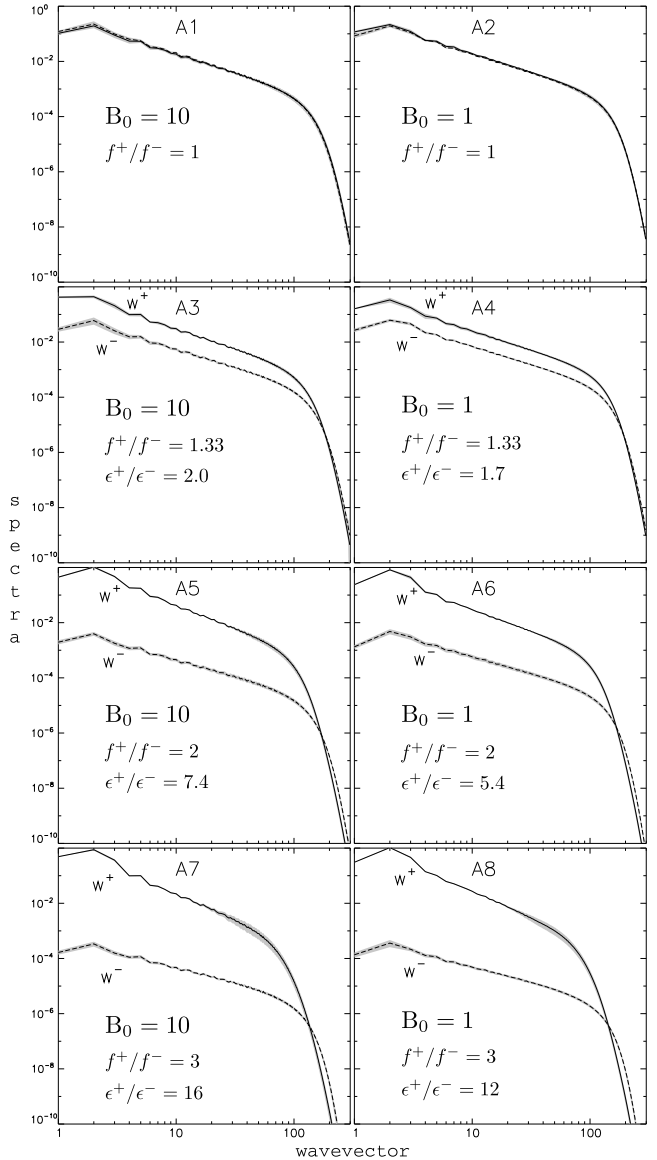


FIG. 9.— Spectra for all data, gray shows mean-square fluctuations in time.

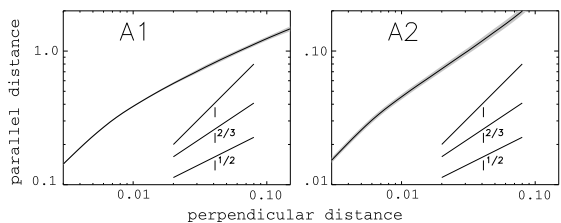


FIG. 10.— Anisotropies for balanced simulations.

called perpendicular spectrum, which takes into account only structures perpendicular to the magnetic field and is the main target of prediction of GS95 model. As they are almost identical we did not have to plot perpendicular spectrum separately. Another definition of spectrum which depend only on the magnitude of the wavevector is the so-called one-dimensional spectrum (see, e.g.



Monin & Yaglom 1965). This spectrum is less sensitive to the bottleneck effect. We refer to the paper of Beresnyak & Lazarian (2008b) (henceforth BL08b) for a more thorough comparison between one-dimensional and 3D spectra and discussion on bottleneck effect.

In Fig. 9, the two bottom plots have relatively large variation (gray areas) on the end of the  $w^+$  spectra. This is due to the fact that in A7 and A8 we barely reached stationary state (for more discussion, see Fig. 4 and §3.2) in the high-resolution run.

Fig. 9 shows spectral slopes between -1.12 and -1.93 with balanced simulations having slopes as flat as -1.37<sup>11</sup>. The GS95 prediction is Kolmogorov's  $-5/3 \approx -1.67$ , while Boldyrev 2006 prediction is -1.5. The flat slopes observed in real data are most certainly due to rather strong bottleneck effect seen in simulations with hyperviscosity. In the imbalanced case the predictions are following: LGS07 predicts -1.67 slopes for all 8 cases; C08 predicts -1.67 for balanced cases A1 and A2, A5-A8 are outside of the applicability of his model, A3 and A4 must show very different slopes – approximately -1 for weak component and -3 for strong component, also C08 predicts pinning on dissipation scales i.e. spectra should converge on dissipation scale<sup>12</sup>. The ratios of the total energies (see Table 1) are predicted as following: C08 – A5-A8 are outside of applicability of his model, A3 and A4 should have very large imbalance  $(w^+)^2/(w^-)^2$  of at least a 1000, while 4-6 is actually observed; LGS07 predicted/observed – A3: 4/5.5, A4: 3/3.9, A5: 55/145, A6: 30/90, A7: 260/1150, A8: 144/1100. We see that in this respect deviations from LGS07 predictions are small for small imbalances but fairly large for large imbalances. BL08a argues that if one drives turbulence with the same anisotropy on outer scale (as in these simulations) the anisotropies of the components will diverge towards small scales, and this solution will not be self-similar (and not power-law). However, BL08a makes predictions regarding *local* slopes even in this case. This can be seen from (1) which is a classic critical balance between weak wave anisotropy and strong wave amplitude and (4) which is strong cascading of the weak wave. We do not expect relations between slopes based on (4) to hold, because it is strongly influenced by bottleneck effect (BL08a also predicts -1.67 slopes for balanced case). However, there is some dependence between energy slope and anisotropy slope, similar to what BL08a predicts. Namely, it follows from (1) that shallower anisotropy slope for  $w^-$  means steeper spectral slope for  $w^+$  which is observed. Also, from (4), steeper spectral slope for  $w^+$  also means shallower spectral slope for  $w^-$  which is also observed.

The anisotropy was measured in the following manner. First, the parallel and perpendicular second order structure functions were calculated, then we found equal values of parallel and perpendicular SFs and in this way the mapping or function between independent variables, parallel or perpendicular scales were created. This function is plotted on Figs 10, 11 with shades of gray indi-

cating RMS fluctuations in time. This definition of  $\Lambda(\lambda)$  mapping can be understood from two-dimensional plot of SF, e.g. Fig. 7, when one follows a contour of SF and finds which parallel scale correspond to particular perpendicular scale. We see that for the imbalanced case anisotropy curves have different slopes and diverge from outer scale where they are equal (this is dictated by driving) to smaller scales where they are different.

We devoted §4 to the discussion of the measurements of the parallel structure function which was used in the above definition of the anisotropy curves. Although it might appear that each and every definition produce a different anisotropy curve, the major difference is between global and local definition of the field direction, while all local methods (“field line”, “model-dependent” and “minimal”), also dubbed “good” in §4, give very similar results. In fact, these is no perceivable qualitative difference between anisotropy curves obtained by either local methods. This could be explained by Fig. 4 middle and bottom panels where the quantitative differences between methods are small, but on the other hand, the dependence of  $SF_{\parallel}$  on scale is strong ( $\sim l_{\parallel}$ ). Also, in the middle panel, the difference is mostly by a constant, which will only give a slight shift of the anisotropy plot. All in all, the claim that anisotropy curves will diverge by a factor of 3 to 4 in strongly imbalanced simulations stay true regardless of the “local” method used. We rejected “global field” method as it does not reveal scale dependent anisotropy – a groundbase of GS95 model. It is worth noting that LGS07, C08 and BL08 use GS95 as a basis and smoothly transit to GS95 in the balanced limit. There is a wealth of theoretical arguments why the SFs has to be measured with respect to the local field (Cho & Vishniac 2000, Maron & Goldreich 2001, etc). We also would like to note that aside from driven simulations described in this paper we also observed a significant difference in  $w^+$  and  $w^-$  anisotropies in a *decaying* imbalanced simulations.

C08 and LGS07 both predict identical GS95 anisotropy for both modes, which is inconsistent with simulations. BL08a predicts diverging anisotropy, most notably, with stronger wave having smaller anisotropy, which is consistent with simulations. The value of the differences, however, do not reach the asymptotic value of  $\epsilon^+/\epsilon^-$  which may be attributed to the short inertial range.

## 6. POLARIZATION ALIGNMENT

Aside from energy-type statistics (second order SFs and spectra) one can measure so-called alignment effects which are, in a sense deviations from the assumptions of independent randomness of fluctuations included in mean-field models. These were discussed in Boldyrev (2005) and numerically discovered for the first time in Beresnyak & Lazarian (2006).

Fig 12. shows two measures of alignment – the angle polarization alignment  $AA = \langle |\sin \theta| \rangle$  (dashed line), where  $\theta$  is an angle between Elsasser variables perturbations  $\delta \mathbf{w}^+ = \delta \mathbf{v} + \delta \mathbf{b}$  and  $\delta \mathbf{w}^- = \delta \mathbf{v} - \delta \mathbf{b}$  and “polarization intermittency”  $PI = \langle |\delta w^+ \delta w^- \sin \theta| \rangle / \langle |\delta w^+ \delta w^-| \rangle$  (solid line).

For the more detailed numerical study of alignment effects we refer to Beresnyak & Lazarian (2006) and BL08b. The potential effect of alignment on the energy cascade was discussed in Boldyrev (2005, 2006), although

<sup>11</sup> The slopes for one-dimensional spectra are steeper, with balanced slope of -1.45 and the most imbalanced slopes -1.97 for strong wave and -1.22 for weak wave

<sup>12</sup> LGS07 does not discuss transition to viscous scales, but, as a model of local cascading, it must have pinning on viscous scale. The pinning, however, is impossible within the framework of LGS07, as the latter predicts  $w^+/w^- = \epsilon^+/\epsilon^-$ .

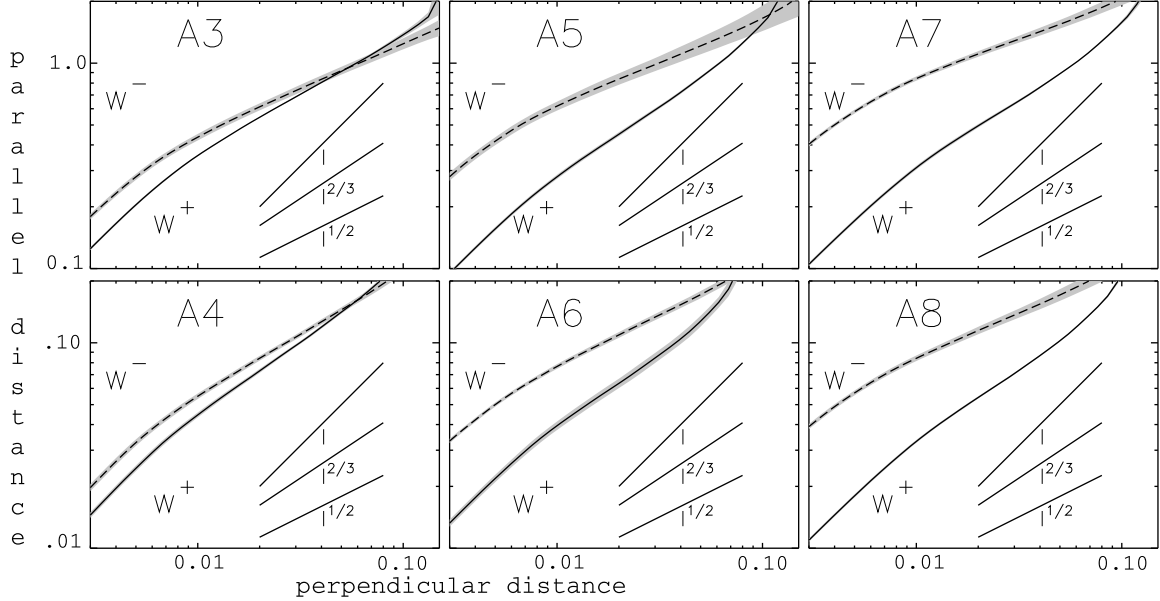


FIG. 11.— Anisotropies for imbalanced simulations. The mapping of  $\Lambda(\lambda)$  is explained in §5. The difference in anisotropy between  $w^+$  and  $w^-$  increases with increasing imbalance.

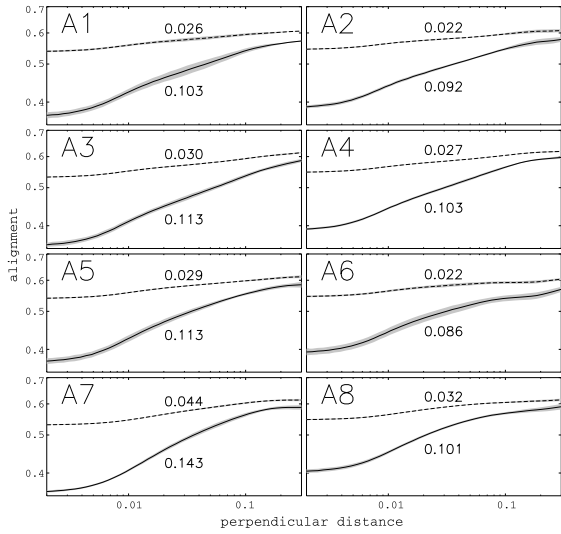


FIG. 12.— Polarization angle alignment (dashed) and polarization intermittency (see definition in the text). Numbers are power-law slopes determined in the middle of the inertial interval.

this effect has not yet been convincingly confirmed by numerics (see BL08b for a discussion and refs).

## 7. DISCUSSION

### 7.1. Comparison with models

We briefly mentioned the tentative nature of *confirming a model* in §1, we also claimed the ability of numerics to *reject some models* on the basis of robust quantities. Although a theory can make a wide variety of predictions, only few of those can be effectively attacked by numerics. One of the quantities that is notoriously hard to measure in DNS is the spectral slope of turbulence. A difference between  $-3/2$  slope and  $-5/3$  can be masked by a variety of effects such as bottleneck effect, driving, and so on. In contrast, the quantities such as Kolmogorov constant are fairly easy to obtain and quickly converge with increasing resolution. In fact, modest resolutions such as

$128^3$  give reasonably precise estimates of this constant. This is due to the fact that the *total energy* and the *total dissipation rate* are easy to measure, to get a statistical average, and also are free of uncertainties of interpretation. What sort of models can be judged on the basis of these quantities? Such are the models of *local cascading* where the cascade rate depend only on the characteristic quantities of, say,  $w_l^\pm$  on a particular scale  $l$  (and, possibly, weakly depend on the spectral slope). In this case numerics only has to reproduce a one or two steps of such cascading to obtain reasonable dissipation rate based on a particular total energy. In this sense our testing does fairly well, as we mostly consider models of local cascading (LGS07, C08, Perez & Boldyrev (2009), Podesta & Bhattacharjee (2009)), at the same time, with  $768^3$  numerical resolution we reproduce five to six binary steps in  $k$ -space.

Our numerical data strongly contradict to three models of imbalanced turbulence, namely LGS07, C08, and Perez & Boldyrev (2009). In particular, two of these models C08, and Perez & Boldyrev (2009) show gross inconsistencies between observed and predicted energy ratios vs dissipation ratios. Indeed, C08 must have a huge energy ratio (of around a 1000) in simulations with  $\epsilon^+/\epsilon^-$  close to two (A3 and A4), while a modest ratios of 4 and 6 are observed. Perez & Boldyrev (2009) does extremely bad in cases with large imbalances. A7 and A8 has an energy ratios of around a 1000, while predicted quantities are 16 and 12. LGS07 does a much better job on energy ratios, but still fails the A7 and A8 (large imbalance) tests, see Fig. 13.

Furthermore, LGS07 and C08 have predictions regarding eddy anisotropies. Both of these models predict equal anisotropies for  $w^+$  and  $w^-$  while a different anisotropies are observed. Aside from these inconsistencies, we also note that C08 predicts pinning at the dissipation scale, which is not observed. C08 also predicts that the strong wave has to have steeper spectral slope than the weak wave. This corresponds to numerics quali-

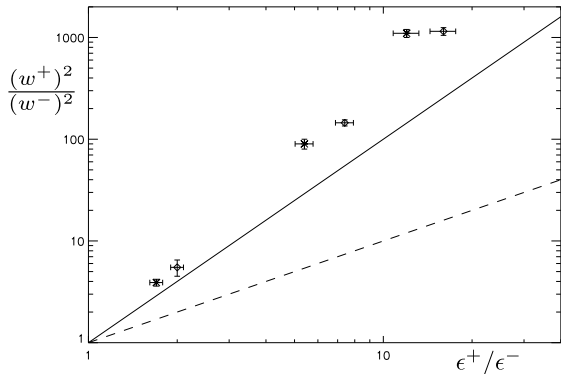


FIG. 13.— Total energy ratio versus dissipation rate ratio (see also Table 1). Diamonds: subAlfvénic simulations, stars: transAlfvénic simulations, solid line: LGS07 prediction, dashed line: Perez & Boldyrev (2009) prediction. There is no simple formula for C08 model, but the energy ratio is expected to become very large when dissipation rate ratio approaches the critical value of around two.

tatively, but not quantitatively, indeed, according to C08, A3 and A4 must have a huge slope difference of around 2, while the real difference is around 0.12.

Although it is harder to confirm a model rather than to reject a model by direct numerical simulations, we see that there is a qualitative agreement between BL08a and numerics. Most of the features predicted by BL08a are observed in simulations, namely a) the anisotropies of the waves are different and strong wave anisotropy is smaller; b) while the weak wave eddies are aligned with respect to the local field on the same scale as the eddy, the strong wave eddies are aligned with respect to a larger-scale field, (Fig. 6); c) the energy imbalance is higher than in the case when both waves are cascaded strongly (Table 1), which suggest that the strong wave is cascaded weakly; d) the dissipation scales for the weak and the strong waves are different, namely the inertial range for weak wave is longer (Fig. 9) which is what predicted by BL08a; e) there is no “pinning” at the dissipation scale which suggest nonlocal cascading.

We note that there is no quantitative agreement between the difference in anisotropies in the “asymptotic power-law solutions” of BL08a and simulations (c.f. §2 and Fig. 11). This is probably due to the fact that asymptotic power-law solutions have not been established within our inertial range.

Aside from three models with detailed strong imbalanced theories that we described above, LGS07, BL08a and C08, recently two papers also made predictions regarding strong imbalanced turbulence. Perez & Boldyrev (2009) predicted that  $(w^+/w^-)^2 = \epsilon^+/\epsilon^-$  which comes to much stronger contradiction with A7 and A8 than LGS07 and as such should be discarded. We note parenthetically that measurements of the stationary levels of energies for  $w^+$  and  $w^-$  are the most robust and model independent of all other measurements. Another paper, by Podesta & Bhattacharjee (2009) is a modification of Perez & Boldyrev (2009) which tries to resolve a huge discrepancy of the latter. Unfortunately, their theory has an arbitrary parameter that can be tuned to change the prediction for  $(w^+/w^-)^2$  and, therefore, it can not be tested numerically. We also note that two aforementioned papers do not have clearly stated predictions for anisotropy, which also limits our ability to test them.

## 7.2. Comparison with earlier simulations

Maron & Goldreich (2001) and Cho et al. (2002) performed 3D numerical simulations of decaying imbalanced turbulence. In these simulations the perturbations obtained as a result of balanced driven MHD modeling were separated into oppositely moving flows of Elsasser variables and one of the flows was arbitrarily decreased in amplitude. The authors observed the increase of the damping time for the strong component. They also observed the increase of turbulence imbalance as the turbulence was evolving. Naturally, no stationary state was achievable for the imbalanced turbulence induced this way.

## 7.3. Role of homogeneous turbulence driving

Properties of imbalanced turbulence may depend on how it is driven. All three major models of imbalanced turbulence that we discuss above (LGS07, BL08a and C08) describe imbalanced turbulence driven homogeneously through the volume. The properties of such turbulence may differ if the sources of driving are localized. To illustrate this fact, in the Appendix A we discuss a toy model of *weak* imbalanced turbulence driven inhomogeneously at boundaries. Note that this approach is very different that the DNS approach of the rest of this paper. Being the model of weak turbulence, this toy model describes only a *perpendicular cascade* just like its predecessor Lithwick & Goldreich (2003), which considered homogeneous case. However, the stationary states of these inhomogeneous and homogeneous cases substantially differ. We also expect to see substantial differences for the homogeneous and inhomogeneous driving for the *strong* imbalanced turbulence, but since such a study with the use of the DNS will be complicated and computationally expensive, we defer this discussion to future publications.

## 7.4. Effects of compressibility

The simulations presented here are of incompressible MHD turbulence. Not only full compressible MHD equations have more degrees of freedom (incompressible approach exclude fast mode perturbations), but compressibility substantially changes the properties of turbulence when sonic Mach numbers are of around unity or higher. However, numerical studies in Cho & Lazarian (2002, 2003) showed that coupling of Alfvénic and magnetosonic waves in strong turbulence is not as strong as was expected, which can be due to the fast non-linear decay of Alfvénic eddies.

In the imbalanced turbulence the strong wave is long-lived. Therefore, one can expect the imbalanced turbulence to be more affected by coupling of incompressible and compressible motions. Density inhomogeneities present in the compressible fluid can act as mirrors reflecting waves and decreasing the degree of turbulence imbalance. Parametric instabilities (see, e.g., Del Zanna et al. 2001) can develop in the compressible fluid, decreasing the imbalance. Thus, stationary states with high degree of imbalance may not be attainable in compressible fluids. Further research in this direction is necessary.

## 8. SUMMARY

In the paper above we have performed MHD numerical simulations of the homogeneously driven imbalanced

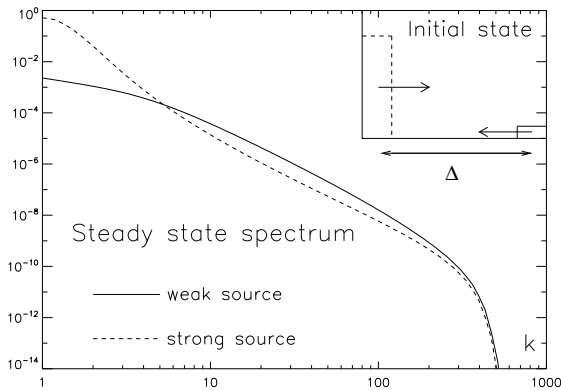


FIG. 14.— Spectrum of up (solid) and downgoing (dashed) waves, in the middle between the wave sources.

turbulence and have shown that:

1. Stationary states exist for rather high degree of imbalance.
2. For large imbalances, the ratio of the amplitudes disagrees with the predictions in LGS07.
3. Rough correspondence of the expectations and measurements are obtained for the model in BL08a, but more studies and testing is necessary.

#### 9. APPENDIX A: INHOMOGENEOUS WEAK IMBALANCED TURBULENCE – A TOY PROBLEM.

Although we understand that the models of imbalanced turbulence are in their making and even the case of homogeneous imbalance turbulence is still being investigated, we decided to add this appendix that probes into a different problem, namely, inhomogeneous Alfvénic turbulence.

This is motivated by the fact that imbalanced turbulence often appears in inhomogeneous setting, i.e. when one has a strong localized source of waves, such as the Sun in solar wind turbulence. In this respect the theory of homogeneous imbalance turbulence should be well-applicable to small scales where the time scales are much smaller than outer timescales. However, on larger scales, homogeneity could be broken. In this section we probe the situation when it is broken. This can be used as a guidance to what extent the observations of the solar wind can be considered as restrictive measurements with respect to the theories of imbalanced turbulence.

Previous studies of weak Alfvénic turbulence (e.g. Galtier et al 2000, Lithwick & Goldreich 2003) considered spatially homogeneous case, which presume that  $w^+$  and  $w^-$  are driven homogeneously in space. This assumption is often violated in nature, specifically when we have a strong directional source of perturbations such as the Sun, which drives one component (let us say,  $w^+$ ) and the other component is being generated at a certain distance from the source by means of, e.g., reflection from density inhomogeneities. This problem is closely related to the problem of the imbalance, however, in most of this paper we considered idealized spatially homogeneous case. Dissipation of waves in turbulence (Beresnyak & Lazarian 2008c) is also related to this problem.

We realize, that by relaxing homogeneity we considerably broaden the physical scope of the model, to the point that we might be unable to draw clear conclusions on the nature of inhomogeneous turbulence. In this situation we preferred to take a first step by considering a

toy problem of weak turbulence with two wave sources separated by a certain distance.

One remarkable new property that could arise from such formulation is that the cascading *might not reach the dissipation scale*. This could happen if, e.g., the sources of the waves are too close to each other. One of the questions that we are asking in this appendix, is whether it is possible that only one wave component, e.g.  $w^-$  is dissipated but the other is simply distorted.

We used simplified equations of weak cascading, the diffusive one dimensional k-space equations for weak perpendicular cascade from Lithwick & Goldreich (2003) which were expanded to one spacial dimension by introducing advection in space, making them an advection-diffusion equations with advection happened in real space, while diffusion represented energy cascading in k-space. We used open boundaries, so that the non-cascaded waves were allowed to freely escape through them.

By solving those equation numerically, changing the distance between wave sources we found that the approximate equality of the energies of the waves at the smallest scale which is reached by cascading is rather robust feature, that is produced by cascading itself. Note that Lithwick & Goldreich 2003 assumed that this “pinning” is due to the dissipation term. In our toy model, however, regardless of whether an actual dissipation took place in the system, the spectra were “pinned” on small scales.

Another possibility that was opened by the inhomogeneous formulation was to drive wave sources with arbitrary power and still obtain a stationary state. In the homogeneous formulation the stationary state was not possible if the rate of energy driving  $\epsilon^+/\epsilon^-$  was larger than 2 (Lithwick & Goldreich 2003). Our inhomogeneous toy model can deal with larger imbalances since the waves were allowed to escape through the open boundaries of the box. Fig. 14 shows spectrum for both types of waves in such case of strong imbalance, and incomplete cascading mentioned above (energy hasn’t reached dissipation scale). Note, that unlike DNS with periodic boundaries from the main body of this paper, where energy can only be lost through dissipation, in this case energy could be lost due to open boundaries and the stationary state could be achieved without any physical dissipation actually taking place.

Fig. 14 demonstrates a feature which was not observed in Lithwick & Goldreich (2003), namely that imbalance reverses on scales an order of magnitude smaller than the driving scale. This unexpected feature is fairly robust in the case “incomplete” cascading and strong imbalance. This suggest that inhomogeneous imbalanced turbulence could be much more complicated that its homogeneous counterpart and further research is necessary.

AB thanks IceCube project for support of his research. AB thanks Teragrid project for providing computational resources. AL acknowledges the NSF grant ATM-0648699, AST-0808118 and the support from the Center for Magnetic Self-Organization in Laboratory and Astrophysical Plasma.

## REFERENCES

- Armstrong, J. W., Rickett, B. J., & Spangler, S. R. 1995, ApJ, 443, 209
- Beresnyak, A., Lazarian, A. & Cho, J. 2005, ApJ, 624, L93-L96
- Beresnyak, A., Lazarian, A. 2006, ApJ, 640, L175
- Beresnyak, A., Lazarian, A. 2008, ApJ, 682, 1070 (BL08a)
- Beresnyak, A., Lazarian, A. 2008, ApJ accepted, arXiv:0812.0812 (BL08b)
- Bigot, B., Galtier, S., Politano, H., Phys. Rev. E, 78, 066301
- Biskamp, D. 2003, *Magnetohydrodynamic Turbulence*. (Cambridge: CUP)
- Boldyrev, S. 2006, Phys. Rev. Lett., 96, 115002
- Chandran, B. D. G. 2008, ApJ, 685, 646
- Cho, J., & Lazarian, A. 2002, Phys. Rev. Lett. 88, 24, 245001
- Cho, J., & Lazarian, A. 2003, MNRAS, 345, 325
- Cho, J., & Lazarian, A. 2004, ApJ, 615, 41
- Cho, J., Lazarian, A., & Vishniac 2002, ApJ, 564, 291
- Cho, J., Lazarian, A., & Vishniac, E. T. 2003, Turbulence and Magnetic Fields in Astrophysics, LNP, 614, 56 (2003b)
- Cho, J. & Vishniac, E., ApJ, 539, 273-282 (2000)
- Del Zanna, L., Velli, M., & Londrillo, P. 2001, A&A, 367, 705
- Dobrowolny, M., Mangeney, A., Veltri, P. 1980, Phys. Rev. Lett., 45, 144
- Elmegreen, B. & Scalo, J., ARA&A, 42, 211 (2004)
- Galtier, S., Nazarenko, S.V., Newell, A.C., Pouquet, A., J. Plasma Phys., 63, 447 (2000)
- Galtier, S., Nazarenko, S.V., Newell, A.C., & Pouquet, A. 2002, ApJ, 564, L49
- Galtier, S., Bhattacharjee, A. 2003, Physics of Plasmas, 10, 3065
- Goldreich, P., & Sridhar, S. 1995, ApJ, 438, 763
- Grappin, R., Pouquet, A., & Leorat, J. 1983, A&A, 126, 51
- Haugen, N. E., Brandenburg, A., Dobler, W. Phys. Rev. E, 70, 016308
- Higdon, J.C. 1984, ApJ, 285, 109
- Howes, G. G., Cowley, S. C., Dorland, W., Hammett, G. W., Quataert, E., Schekochihin, A.A. 2006, ApJ, 651, 590
- Howes, G. G., Dorland, W., Cowley, S. C., Hammett, G. W., Quataert, E., Schekochihin, A.A., Tatsuno, T. 2008, Phys. Rev. Lett., 100, 065004
- Iroshnikov, P.S. 1963, AZh, 40, 742
- Kolmogorov, A. 1941, Dokl. Akad. Nauk SSSR, 31, 538
- Kraichnan, R.H. 1965, Phys. Fluids, 8, 1385
- Lazarian, A. 2009, Space Science Reviews, 143, 357
- Lithwick, Y., & Goldreich, P. 2001, ApJ, 562, 279
- Lithwick, Y., & Goldreich, P. 2003, ApJ, 582, 1220
- Lithwick, Y., Goldreich, P., & Sridhar, S. 2007, ApJ, 655, 269
- Maron, J., & Goldreich, P. 2001, ApJ, 554, 1175
- McKee, C. F., & Ostriker, E. C. 2007, ARA&A, 45, 565
- Matthaeus, W.M., Goldstein, M.L., Montgomery, D.C. 1984, Phys. Rev. Lett., 51, 1484
- Matthaeus, W. H., & Montgomery, D. 1980, New York Academy Sciences Annals, 357, 203
- Monin, A.S., Yaglom, A.M. 1975, *Statistical Fluid Mechanics: Mechanics of Turbulence*, NY: Dover
- Montgomery, D.C., & Turner, L. 1981, Phys. Fluids, 24, 825
- Müller, Grappin 2005, Phys Rev Lett 95, 114502
- Müller W.-C., Biskamp, D., & Grappin, R 2003, Phys. Rev. E, 67, 066302
- Ostriker, E. C., Stone, J. M., & Gammie, C. F. 2001, ApJ, 546, 980
- Perez, J., Boldyrev, S. 2009, Phys. Rev. Lett., 102, 025003
- Podesta, J. J.; Bhattacharjee, A. 2009, arXiv:0903.5041
- Pouquet, A., Frisch, U., Leorat, J. 1976, J. of Fluid Mech., 77, 321
- Pouquet, A., Sulem, P. L., Meneguzzi, M. 1988, Phys. of Fluids, 31, 2635
- Roberts, D. A., Goldstein, M. L., Klein, L. W., Matthaeus, W. H. 1987, J. of Geophys. Res., 92, 12023
- Schekochihin, A.A., Cowley, S. C.; Dorland, W., Hammett, G. W., Howes, G. G., Quataert, E., Tatsuno, T. 2007, arXiv:0704.0044
- Shebalin, J.V., Matthaeus, W.H., & Montgomery, D. 1983, J. of Plasma Phys., 29, 525
- Stone, J.M., Ostriker, E.C., Gammie, C.F. 1998, ApJ, 508, L99
- Vázquez-Semadeni, E., Gómez, G. C., Jappsen, A. K., Ballesteros-Paredes, J., González, R. F., & Klessen, R. S. 2007, ApJ, 657, 870
- Vogt, C., & Enßlin, T. A. 2005, A&A, 434, 67